Thermal effects on creep of sensitive clay slopes

Citation for the original published paper (version of record):
Cheng, X., Abed, A., Karstunen, M. (2025). Thermal effects on creep of sensitive clay slopes. IOP Conference Series: Earth and Environmental Science, 1523(1).
http://dx.doi.org/10.1088/1755-1315/1523/1/012011

IOP Conference Series:
Earth and
Environmental Science

PAPER • **OPEN ACCESS**

Thermal effects on creep of sensitive clay slopes

To cite this article: Xiaoyang Cheng *et al* 2025 *IOP Conf. Ser.: Earth Environ. Sci.* **1523** 012011

IOP Conf. Series: Earth and Environmental Science **1523** (2025) 012011 doi:10.1088/1755-1315/1523/1/012011

Thermal effects on creep of sensitive clay slopes

Xiaoyang Cheng[1*], Ayman Abed[1] and Minna Karstunen[1]

[1] Department of Architecture and Civil Engineering, Chalmers University of Technology, Gothenburg, Sweden

[*]E-mail: chengxi@chalmers.se

Abstract. The slopes in soft clays typically exhibit creep movements due to their viscous behavior under gravity. Temperature plays a key role in controlling the creep rate. To date, there are limited studies on the thermal effect on creep movement of sensitive clay slopes. This paper employs a thermal-hydro-mechanical numerical code to investigate the thermal response of a clay slope under yearly thermal cycles ranging from 0.5 ℃ to 19.1 ℃. The thermo-viscoplastic Creep-SCLAY1ST constitutive model is adopted to capture the evolution of preconsolidation pressure with temperature. The results are compared to those under constant temperature conditions, in terms of creep movements and stress paths for soil elements at different locations of the slope. The results of this work aim to draw attention to the role of temperature in the assessment of long-term slope stability, especially for slopes in sensitive clay.

1. Introduction

In recent years, slopes have been increasingly exposed to extreme environmental events due to climate change. The rapid landslides reported by e.g. [1], [2], [3] suggest that thermal effects might play a major role. Numerous studies have shown that temperature fluctuations, even in temperature ranges naturally experienced on the ground surface, can impose hydromechanical forces, which affect hydraulic conductivity, water retention capacity, compressibility and mobilized shear strength [4, 5, 6, 7]. A better understanding of the thermal-hydro-mechanical (THM) behavior of soils, is necessary for the design or assessment of both cut (man-made) and natural slopes.

Despite various studies on the effects of THM coupling on slope stability, few works have investigated thermal effects on the long-term behavior, especially for slopes in sensitive natural clays, similar to those in Canada and Scandinavia, associated with creep movements. It is generally recognized that the creep of clays with time can lead to displacements and a reduction of the undrained shear strength, which may result in the prefailure stage of the slope that occurs before a first-time failure described by [8], jeopardizing the long-term stability of slopes in soft sensitive clay. A recent experimental work by [9] revealed a significant temperature effect on the creep rate of natural sensitive clays at stress levels near the apparent preconsolidation pressure on moderate temperature variations (5 ℃ to 25 ℃). Similarly, [10] reported a notable increase in the creep index (C_α) especially at higher stress levels and temperatures in the post-yield region. These findings highlight the importance of understanding the thermal behavior of creep movements of slopes in sensitive clay.

Simulating the creep movement of a clay slope considering the THM coupling effect is challenging, as it requires: i) a robust constitutive model; and ii) computational efficiency for a

long-term period. Various researchers [11, 12, 13, 14, 15, 16] have proposed different constitutive models based on experimental observations. Most of them focus on the influence of large temperature amplitude resulting from nuclear waste barriers. This research has used an advanced finite element model to examine the influence of temperature on the creep movement of a slope in sensitive clay. The adopted model employs a coupled THM framework integrated with a newly developed Creep-SCLAY1ST model [17, 18] to accurately predict the rate and temperature dependent behavior of sensitive clay. By analyzing the temperature-dependent deformation response, we aim to provide insight into the potential risks posed by thermal variations to the assessment of slope movements.

2. Governing balance equations

This section briefly presents the governing balance equations for water mass, thermal energy and linear momentum with assumptions: (1) the porous geomaterial consists of three phases - liquid (l), gas (g) and solid (s); (2) solid phase does not dissolve or sublimate while water may transform between vapour and liquid; (3) dry air is not considered.

2.1 Water mass balance equation

The mass balance equation for water component is presented by:

$$\begin{aligned}&[n(\rho_w^l-\rho_w^g)\frac{\delta S^l}{\delta T}-(1-n)(S^l\rho_w^l+S^g\rho_w^g)\beta_{sT}-nS^l\beta_{wT}\rho_w^l\\&\qquad+nS^g\frac{\rho_w^g}{T^2}(4974+\frac{M_w\Psi}{R\rho_w^l})]\frac{\partial T}{\partial t}\\&+[nS^l\beta_{wp}\rho_w^l+nS^g\frac{\rho_w^gM_w}{\rho_w^lRT}-n(\rho_w^l-\rho_w^g)\frac{\partial S^l}{\partial\Psi}]\frac{\partial u_w}{\partial t}\\&+(S^l\rho_w^l+S^g\rho_w^g)\frac{\partial\varepsilon_v}{\partial t}+\boldsymbol{\nabla}\cdot[\frac{K_w}{\rho_w^lg}(\nabla u_w+\rho_w^l\mathbf{g})]=0\end{aligned}\tag{1}$$

where n is the soil porosity, ρ_w^l is the water density in a liquid phase dependent on the pore water pressure u_w and the temperature T, ρ_w^g is the vapour density in a gas phase. S^l and S^g are the degree of saturation for liquid and gas, respectively, where S^l is assumed to be a simple function of suction Ψ for unsaturated soil [19]. β_{sT} and β_{wT} are the coefficients of volumetric thermal expansion in solids and water, respectively. β_{wp} is the coefficient of compressibility of the water, ε_v is the volumetric strain. M_w is the molar mass of vapour and R is the universal gas constant. K_w denotes hydraulic conductivity of liquid water and $\mathbf{g}$ is gravity vector.

2.2 Thermal energy balance equation

The balance equation of thermal energy considering the latent heat of vaporization and heat due to conduction and convection can be expressed as:

$$\underbrace{\frac{\partial\Phi_h}{\partial t}}_{\text{heat storage}}+\underbrace{L\dot{Q}_w^g}_{\text{latent heat of vaporization}}+\underbrace{\boldsymbol{\nabla}\cdot\mathbf{q_h}}_{\text{heat due to conduction and convection}}=0\tag{2}$$

where L is the latent heat of vaporization. The soil heat capacity Φ_h, the rate of vapour production $\dot{Q}_w^g$ and the heat flux $\mathbf{q_h}$ are defined as Eqs. 3, 4 and 5.

$$\Phi_h=[(1-n)\rho^sc_s+nS^l\rho_w^lc_w^l+nS^g\rho_w^gc_w^g](T-T_0)\tag{3}$$

$$\dot{Q}_w^g = -(1-n)S^g\rho_w^g\beta_{sT}\frac{\partial T}{\partial t} + S^g\rho_w^g\frac{\partial \varepsilon_v}{\partial t} - n\rho_w^g\frac{\partial S^l}{\partial t} + nS^g\frac{\partial \rho_w^g}{\partial t} \quad (4)$$

$$\mathbf{q}_{\mathrm{h}} = -\lambda_T\nabla T + \frac{\rho_w^l c_w^l K_w}{\rho_w^l g}(\nabla u_w + \rho_w^l \mathbf{g})(T - T_0) \quad (5)$$

where c_w^l and c_w^g are the specific heat capacity of water components in liquid phase and gas phase, respectively. T_0 is the reference temperature with a value of 293.16 K for this research. λ_T is the thermal conductivity.

2.3 Mechanical balance equation

The mechanical balance equation is given by:

$$\boldsymbol{\nabla}\cdot\boldsymbol{\sigma}^{\mathrm{tot}} + \mathbf{b} = 0 \quad (6)$$

where $\boldsymbol{\sigma^{tot}}$ is the total stress tensor, $\mathbf{b} = \rho^b\mathbf{g}$ is body force that typically denotes self-weight of material related to its bulk density. In this research, the mechanical behaviour is described by the Creep-SCLAY1ST model [17, 18], which builds upon Creep-SCLAY1S model [20] capable of capturing the rate dependency, anisotropy and destructuration, but enhanced with an additional temperature dependent surface (TDS) to simulate the change in creep rate of clay observed under thermal loading. Thus, four surfaces are used to describe the state of soil, including Normal Consolidation Surface (NCS), Current Stress Surface (CSS), Intrinsic Compression Surface (ICS) and Temperature Dependent Surface (TDS), as illustrated in p'-q stress space in Fig. 1. The NCS distinguishes small and large creep strain rates, being defined by the pre-consolidation pressure p'_m. CSS represents the current mean effective stress state and is defined by the mean hydrostatic effective stress p'_{eq}. The ICS representing an unbonded soil with the same void ratio is introduced to account for the bonding effect, whose size is defined by the intrinsic isotropic preconsolidation pressure p'_{mi}. The TDS tracks the evolution of ICS under different thermal loading. The size of TDS is determined by the p'_T. Details can be found in [17] and [18].

The corresponding weak formulation and FE discretization of the balance equations (Eqs. 1, 2 and 6) can be derived by applying the standard finite element discretization method (see details in [21]). The proposed numerical framework has been implemented on the open source computational platform FEniCS [22], with applicability to capture the hydromechanical (HM) and thermal-hydro-mechanical (THM) behavior of partially saturated soil recently demonstrated by [18] and [23]. In this study, the model is employed to conduct numerical analyses to investigate the importance of temperature-induced changes in slope movements in sensitive clay.

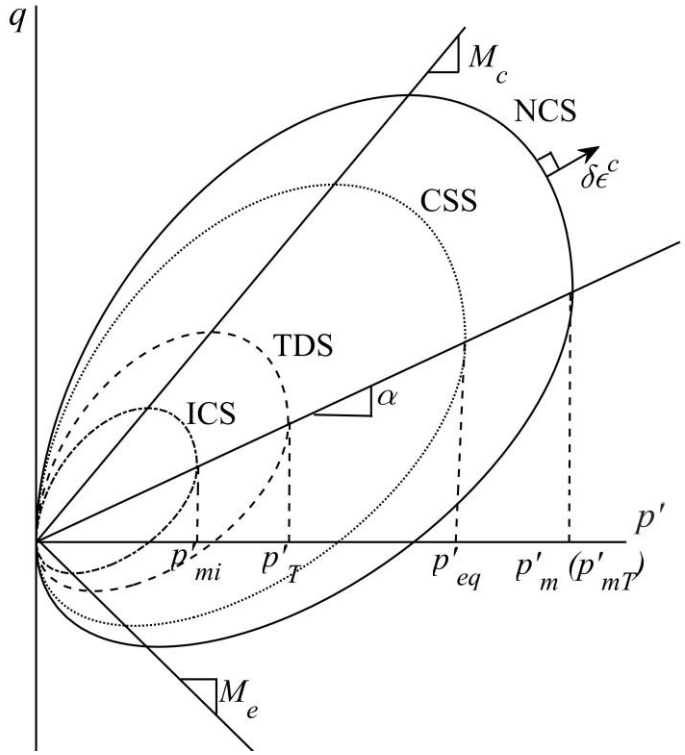

Figure 1. Reference surfaces of Creep-SCLAY1ST model.

3. Numerical simulation

3.1 Numerical model setup

A two-dimensional (2D) slope with a horizontal length of 20 m, crest height of 10 m and inclination of 3V:4H is created. The geometry and the FE mesh used for the numerical model are depicted in Fig. 2. Note that this is an arbitrary slope for the purpose of analysis. A local refinement of mesh near the slope surface is adopted to obtain more precise results. The bottom of the domain is fixed in all directions, while no horizontal movement is allowed for the lateral boundaries. The model is capable of simulating different water tables. Herein, a constant water table is established through the toe of the slope. The lateral sides of the model are set as impermeable boundaries. The initial ground temperature is set to 8.7 ℃. The thermal cycles are simulated using a time-dependent prescribed temperature as a thermal boundary condition at the top surface of the soil domain (Fig. 2), whereas the bottom and lateral boundaries were set to thermally insulated.

The parameters of the Creep-SCLAY1ST model used for the simulation are summarized in Table 1. Detailed calibration procedures are discussed in [20]. The parameters for the hydraulic and thermal material properties are listed in Table 2.

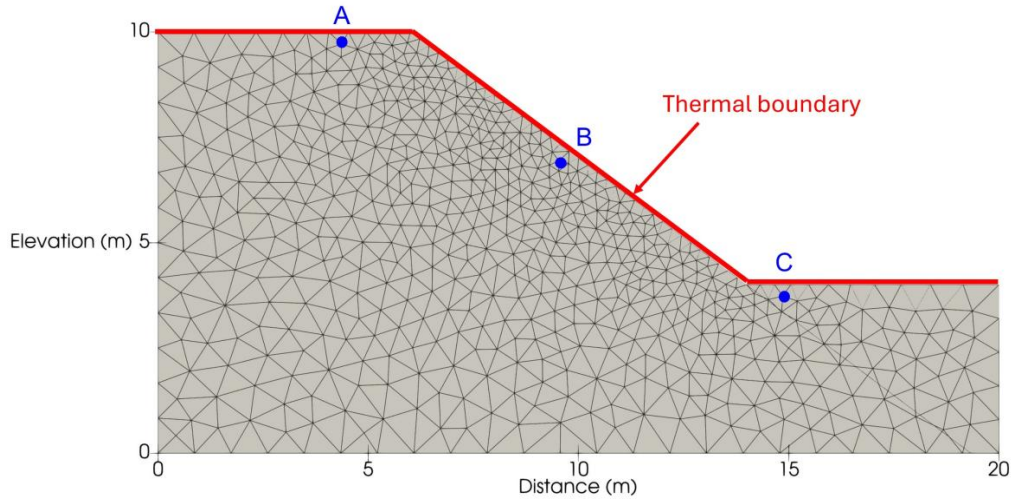

Figure 2. Representative mesh used in the simulations.

Table 1. Mechanical parameters for Creep-SCLAY1ST.

Description		Parameter	Value
Initial state variable	Initial void ratio	e_0	1.9
	Overconsolidation ratio	OCR	1.2
	Initial anisotropy	α_0	0.5
	Initial amount of bonding	χ_0	6
	Reference temperature (°C)	T_{ref}	7
Isotropic stiffness parameters	Modified intrinsic compression index	λ*	0.0862
	Modified swelling index	κ*	0.0083
	Poisson's ratio	ν'	0.25
Creep parameters	Modified intrinsic creep index	μ'	0.004
	Reference time (days)	τ	1
Critical state parameters	Stress ratio at critical state in compression	M_c	1.45
	Stress ratio at critical state in extension	M_e	1.1
Anisotropy parameters	Rate of rotational hardening	ω	40
	Relative deviatoric rate of rotational hardening	ω_d	0.9
Bonding parameters	Rate of destructuration	ξ	9
	Relative deviatoric rate of destructuration	ξ_d	0.3
Thermal parameters	Thermal rate of change in preconsolidation pressure	a_T	0.0085
	Intrinsic thermal constant for preconsolidation pressure	b_T	0.0051

Table 2. Parameters for balance equations.

(a) Hydraulic properities				
S_{res}^{l}	S_{sat}^{l}	k_{sat}^{l} (m²/s)		
0.23	1	3.5×10^{-17}		
(b) Thermal properities				
λ_T (W/m/K)	c_s (J/kg/K)	c_w^l (J/kg/K)	c_w^g (J/kg/K)	
1.17	3300	4180	1900	
(c) Phases properties				
ρ_{w0}^{l} (kg/m³)	ρ_s (kg/m³)	β_{wp} (1/pa)	β_{sT} (1/K)	β_{wT} (1/K)
1000	2650	4.58×10^{-10}	7.8×10^{-6}	2.1×10^{-4}

The following steps are used in the FE analyses to investigate the thermal effect on slope movement:

- Geostatic step. The model with the horizontal ground surface attains equilibrium under its self-weight.
- Formation of the slope. Taking into account natural geological erosion processes, the slope geometry presented in Fig. 2 is obtained by progressively unloading the previously mentioned model to obtain accurate values for the initial state variables of the Creep-SCLAY1ST model.
- Initialization of temperature. The input data are represented by the monthly average air temperature ranging from 0.5 °C to 19.1 °C, recorded in Gothenburg in 2018 [24], as indicated by the red squares in Fig. 3. The initial temperature is 8.7 °C for the whole soil domain. Then the temperature on the top surface is reduced to 0.5 °C corresponding to the initial temperature recorded in the field in January, as indicated by the dashed line in Fig. 3
- Thermal cycles. To evaluate the long-term creep movement of the clay slope, the measured temperature is repeated for a scenario of 5 years and is applied to the model in the manner described previously. The calculated temperature on the surface compares well with the measurement, as shown in Fig. 3.

3.2 Results

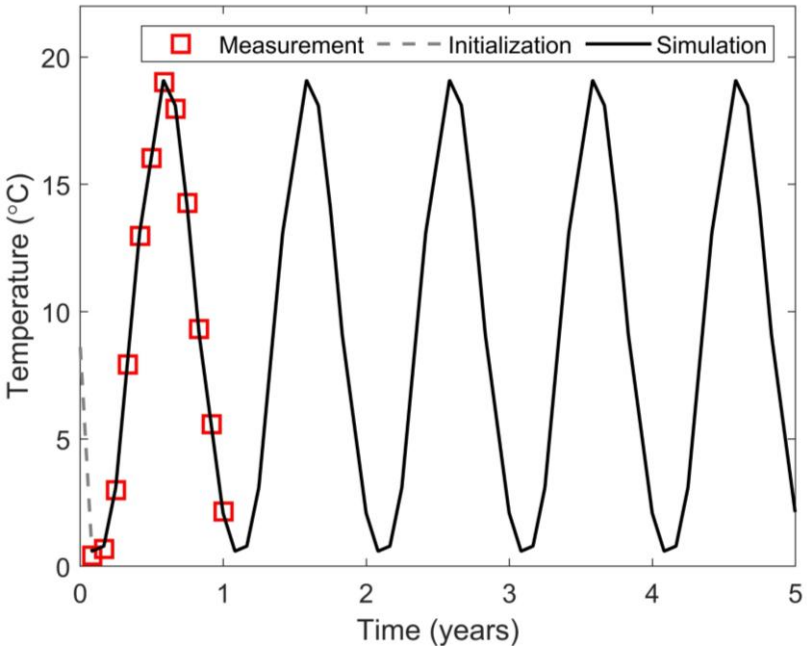

Figure 3. Variation of temperature on the surface of slope.

Fig. 4 presents the evolution of temperature and total displacement throughout the thermal cycles. The subfigures illustrate the conditions at the start of the thermal cycles (Fig. 4a), the peak (Fig. 4b) and end (Fig. 4c) of the first cycle, and the end of the last cycle (Fig. 4d). The first column displays the temperature distribution, while the second shows the total displacement and the nodal displacement vectors under thermal boundary conditions. Note that the length of the vector does not indicate the magnitude of the displacement. For comparison, the displacement without thermal boundary effects is also included in the third column. It can be clearly observed in Fig. 4 that vertical displacement is dominant for the soil in the area without unloading. The soil primarily moves downward along the slope surface. The soil near the toe of the slope moves horizontally most of the time, while the soil in the far field displays an upward direction. The contours indicate that the amplitude of soil displacement increases over time, with the most significant settlement occurring at the crest of the slope and the smallest at the toe. The difference between cases with and without thermal boundary conditions seems negligible. This result is expected because clay with low initial bonding (χ_0= 6) is less sensitive to a temperature change [9].

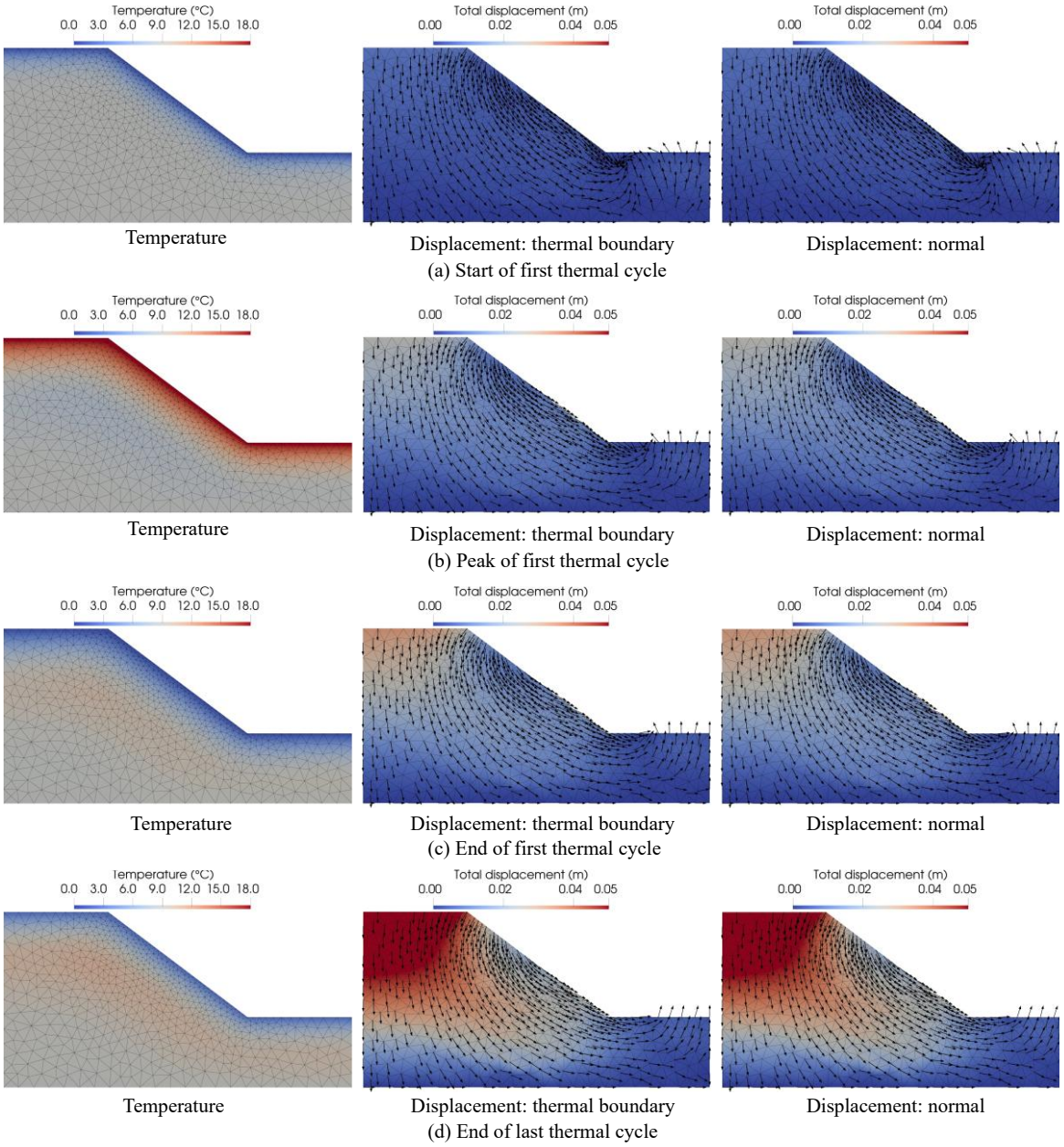

Figure 4. Temperature and displacement at (a) start of first thermal cycle; (b) peak of first thermal cycle; (c) end of first thermal cycle; (d) end of last thermal cycle.

Further inspection of displacement is provided in Fig. 5 by showing the evolution of displacements with time at three reference soil elements - Element A, B and C that are defined along the subsurface in Fig. 2. Fig. 5 compares the horizontal and vertical displacements for the cases with and without thermal boundary and initial bonding χ_0 = 6 and χ_0 = 20 are considered. The vertical red line denotes the start of thermal cycles. As expected, no significant difference in displacement is observed for all reference elements when considering the thermal boundary for χ_0 = 6 in Figs. 5a and 5b, again demonstrating that the temperature variation has limited influence on the creep for clay with lower sensitivity (less structure). It is observed in Figs. 5c and 5d that

Element A develops a higher displacement under thermal cycles than that under constant ground temperature for χ_0 = 20, while the effect of varied temperature on the displacements at Element B and C is invisible. Such behavior is directly related in the Creep-SCLAY1ST model to the overconsolidation ratio (OCR* = $\frac{p'_m}{p'_{eq}}$), with the assumption that heavily overconsolidated soil exhibits small creep strains. Fig. 6 depicts the time evolution of OCR* at the selected elements. It can be seen that the highest OCR* value appears at Element C, the second highest appears at Element B, followed by the third at Element A attributed to their extent of unloading during slope formation. The cyclic amplitude of OCR* is much higher for χ_0 = 20 than for χ_0 = 6. The cyclic variation of OCR* reveals that the Creep-SCLAY1ST model can satisfactorily capture the evolution of preconsolidation pressure under different thermal loads.

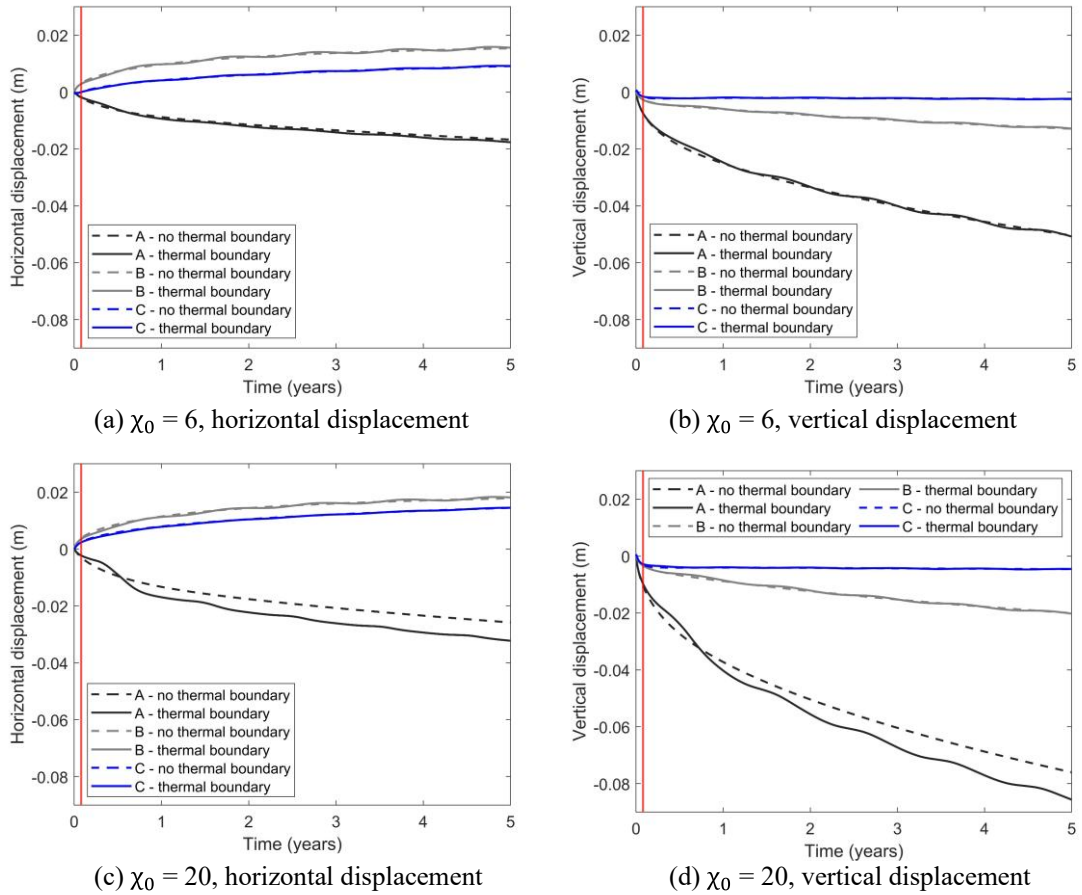

(a) χ_0 = 6, horizontal displacement (b) χ_0 = 6, vertical displacement

(c) χ_0 = 20, horizontal displacement (d) χ_0 = 20, vertical displacement

Figure 5. Displacement of reference elements: (a) horizontal displacement for χ_0 = 6; (b) vertical displacement for χ_0 = 6; (c) horizontal displacement for χ_0 = 20; (d) vertical displacement for χ_0 = 20.

The thermal strain of soil is greatly dependent on the OCR*. Fig. 7 presents the change in the volumetric strain ε_v of reference elements during thermal cycles for χ_0= 6, in which the square represents the state after unloading and the dashed line represents the temperature initialization stage. The negative sign of ε_v stands for contraction. The slightly overconsolidated Element A (OCR* = 1.3) generally shows an irreversible contraction under heating and expansion during

cooling, while heavily overconsolidated Element C (OCR* = 5) exhibits reversed change during the thermal cycles in a nearly elastic manner. Notably, the result is generally consistent with the findings by [25] and [26]. However, compared to the experimental results for normally consolidated clay, Element A develops a higher volumetric strain during the cooling of the first cycle, which is caused by the low frequency of thermal cycles (1 year) and therefore more creep strain accumulates. Due to the movement of the surrounding soil, the overconsolidated Element B with OCR* = 4 does not show a typical thermo-elastic response.

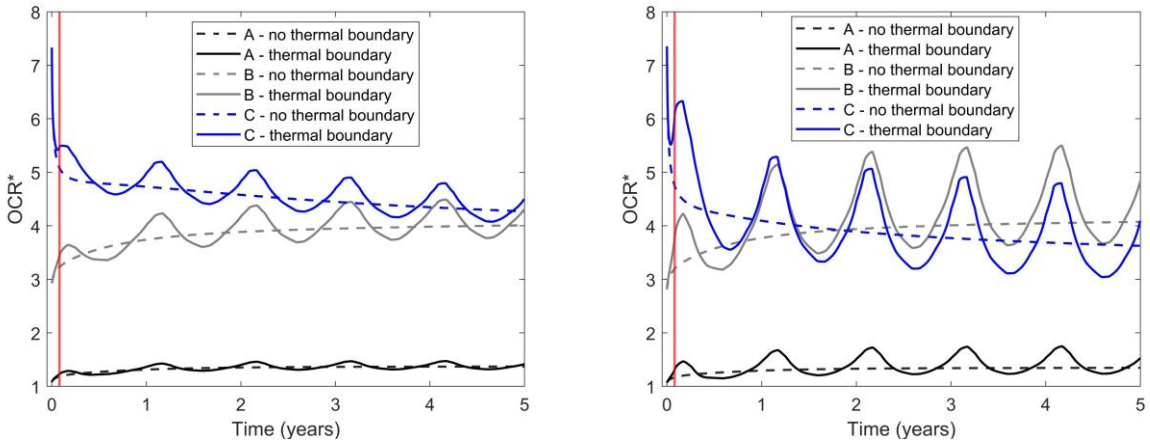

Figure 6. Overconsolidation ratio (OCR*) of reference elements for: (a) χ_0 = 6; (b) χ_0 = 20.

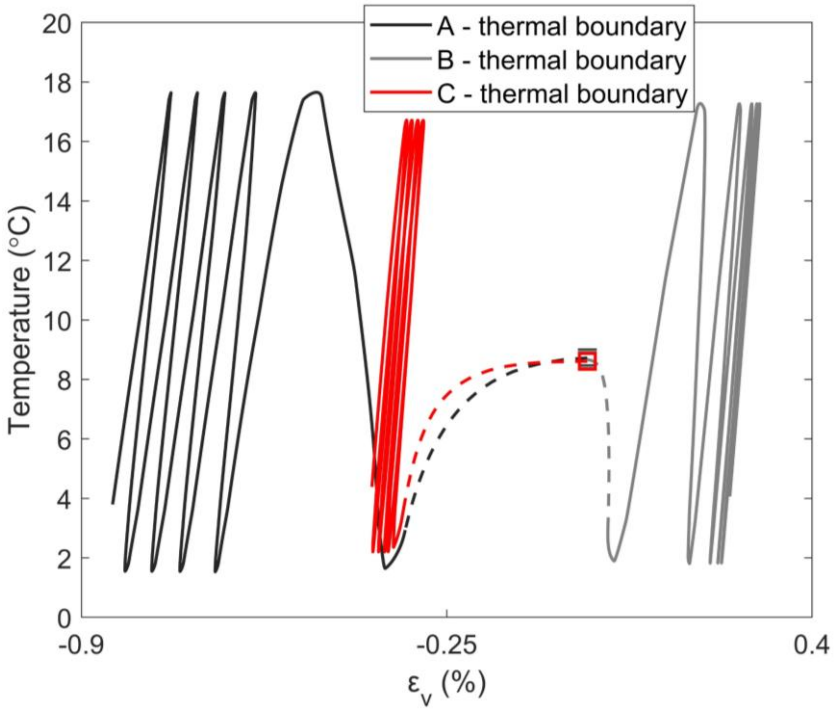

Figure 7. Volumetric strain during thermal cycles.

It is interesting to show how the stress paths evolve with time. Figs. 8 and 9, respectively, display the cyclic stress path of the reference elements in terms of deviatoric (q) and mean effective (p') stresses for χ_0 = 6 and χ_0 = 20, with the colour sidebars indicating the evolution of temperature. The stress path obtained without temperature variation (black dashed line) is also included. The square marker represents the state after unloading, while the triangle marker stands for the start of thermal cycles. The stress paths during the temperature initialization stage (from the square to the triangle marker) nearly superpose for both cases with and without thermal boundaries for all the reference elements. Afterwards, although the overall trends of the two cases are similar, the stress paths under thermal cycles can be observed to progress at a gradually decreasing rate. Figs. 8 and 9 clearly show that the stress path depends on the specific location of each reference element, as summarized as follows:

- Element A. In Figs. 8a and 9a, the element experiences an increase in deviatoric stress and a decrease in mean effective stress. That is the result of the relaxation of horizontal stress induced by the right downward movement of the soil on the crest. Despite the continuous variation of temperature within each cycle, the significant increase in the deviatoric stress level occurs at the lowest temperature.
- Element B. A drastic reduction in deviatoric stress during the temperature initialization state is observed in Figs. 8b and 9b, and then the stress is maintained nearly constant with a gradual decrease in p'. The horizontal stress path suggests an isotropic unloading behaviour.
- Element C. Different from Element A and B, the increase in the mean effective stress p' arises during the temperature initialization stage. As the thermal cycles process, the stress path may cyclically evolve towards (nearly) isotropic conditions under a constant p' (Fig. 8c), while an extension state is reached for χ_0 = 20 (Fig. 9c).

4. Conclusion

In this research, a THM coupled numerical code combined with the thermo-viscoplastic Creep-SCLAY1ST model was employed to investigate the response of a sensitive clay slope to thermal cycles. The slope was created by unloading a horizontally layered model to obtain the accurate initial state variables for Creep-SCLAY1ST. A parametric study on different initial bonding parameters (i.e. initial sensitivity) was carried out by examining the behavior of soil elements at different locations in the vicinity of the slope. Compared to the results without temperature variation, the following key conclusions were drawn:

- Thermal cycles have limited influence on creep movement of slopes in the low sensitivity clay, whereas for a moderately sensitive clay these effects cannot be ignored.
- The largest vertical settlement appears at the crest of the slope, while the smallest settlement appears at the toe of the slope, which is mainly linked to the loading history (OCR).
- The thermal volumetric response in Fig. 7 confirms the experimental observations from soil element tests that the overconsolidated clay shows thermo-elastic response, while the normal consolidated or slightly overconsolidated clay undergoes volumetric contraction during heating and dilation during cooling. However, for the boundary value problem, the movement of the surrounding soil should be considered.
- The cyclic stress path induced by the thermal cycles has a similar trend to that under constant temperature.

The presented numerical study has demonstrated the capability of the numerical code to capture the thermal behavior of clay. The findings will contribute to the development of improved stability assessments and mitigation strategies for sensitive clay slopes exposed to thermal influences. Future work will be extended to explore: i) a real slope, ii) thermal response of slope for a longer term, and iii) response under extreme climate conditions.

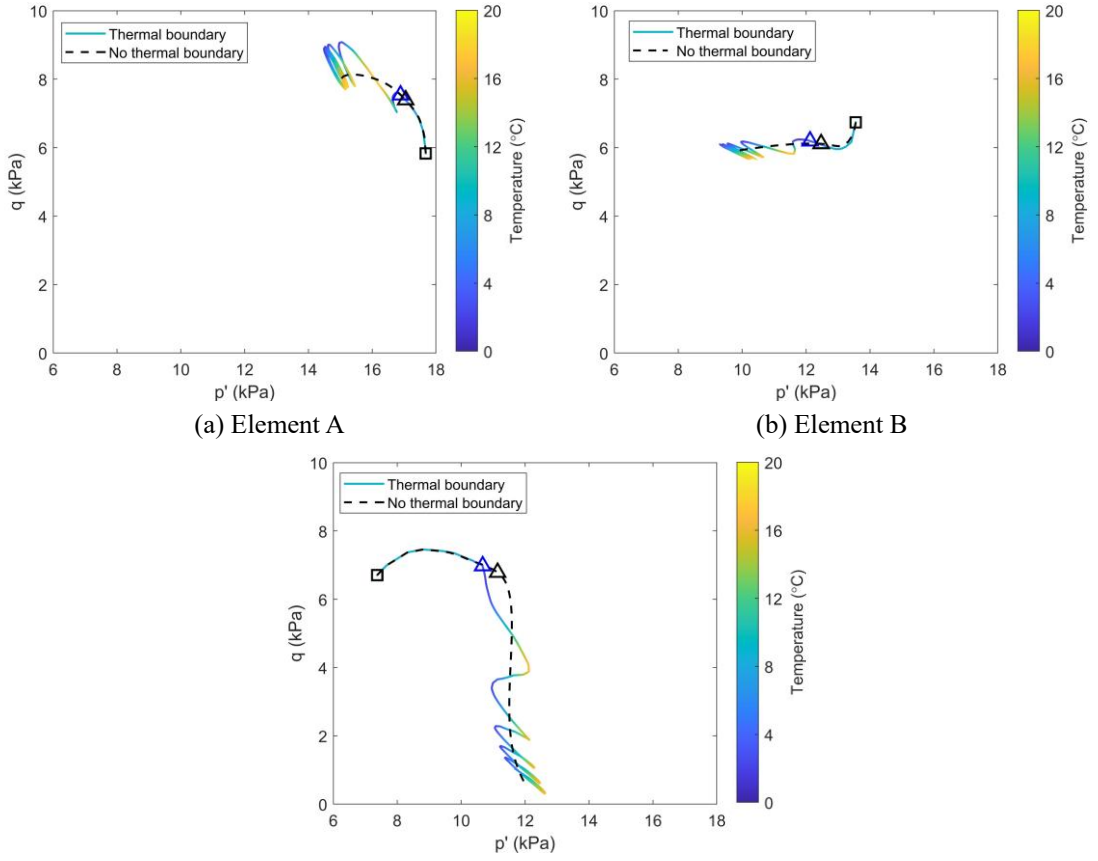

(a) Element A (b) Element B

(c) Element C

Figure 8. Stress path in $p' - q$ space for χ_0 = 6 at: (a) Element A; (b) Element B; (c) Element C. Note: Square marks the stress state after unloading and triangle marks where thermal cycles start.

Acknowledgements

The work is funded by Formas (Research Council for sustainable Development) (Grant 2021-02400), Swedish Research Council (VR 2024-04672) and Swedish Transport Administration (Grant 2022/69758) via BIG (Branchsamverkan in grunden). The work is done as part of Digital Twin Cities Centre that is supported by Sweden's Innovation Agency VINNOVA (Grant 2024-03904).

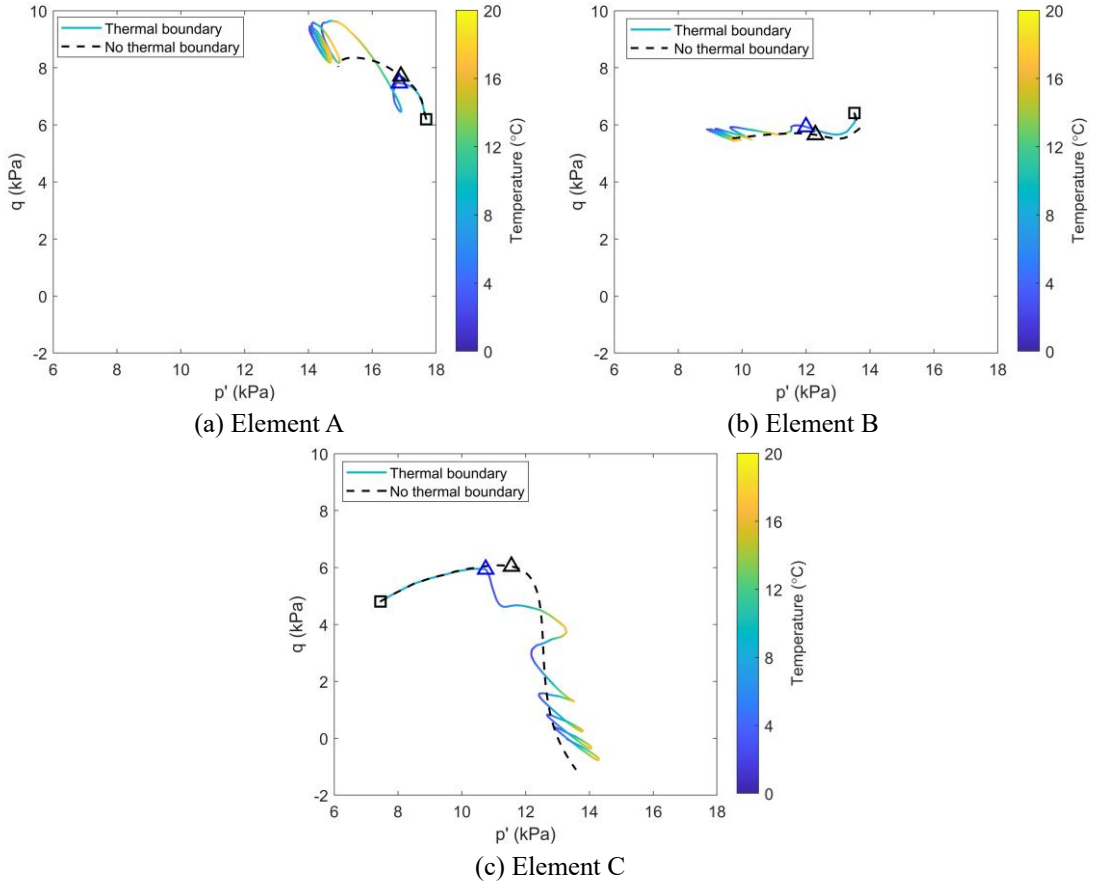

(a) Element A (b) Element B

(c) Element C

Figure 9. Stress path in $p' - q$ space for χ_0 = 20 at: (a) Element A; (b) Element B; (c) Element C.
Note: Square marks the stress state after unloading and triangle marks where thermal cycles start.

References

[1] Pinyol, N.M. and Alonso, E.E., 2010. Criteria for rapid sliding II.: Thermo-hydro-mechanical and scale effects in Vaiont case. *Engineering Geology*, *114*(3-4), pp.211-227.
[2] Alonso, E.E., Zervos, A. and Pinyol, N.M., 2016. Thermo-poro-mechanical analysis of landslides: from creeping behaviour to catastrophic failure. *Géotechnique*, *66*(3), pp.202-219.
[3] Seguí, C., Rattez, H. and Veveakis, M., 2020. On the stability of deep-seated landslides. The cases of Vaiont (Italy) and shuping (Three Gorges Dam, China). *Journal of Geophysical Research: Earth Surface*, *125*(7), p.e2019JF005203.
[4] Delage, P., Sultan, N., Cui, Y.J. and Ling, L.X., 2011. Permeability changes in Boom clay with temperature. *arXiv preprint arXiv:1112.6396*.
[5] Leroueil, S., 1996. Compressibility of clays: fundamental and practical aspects. *Journal of geotechnical engineering*, *122*(7), pp.534-543.
[6] Pham, T.A., Hashemi, A., Sutman, M. and Medero, G.M., 2023. Effect of temperature on the soil–water retention characteristics in unsaturated soils: Analytical and experimental approaches. *Soils and Foundations*, *63*(3), p.101301.
[7] Garcia, L.M., Pinyol, N.M., Lloret, A. and Soncco, E.A., 2023. Influence of temperature on residual strength of clayey soils. *Engineering Geology*, *323*, p.107220.

[8] Leroueil, S., 2001. Natural slopes and cuts: movement and failure mechanisms. *Géotechnique*, *51*(3), pp.197-243.
[9] Li, Y., Dijkstra, J. and Karstunen, M., 2018. Thermomechanical creep in sensitive clays. *Journal of Geotechnical and Geoenvironmental Engineering*, *144*(11), p.04018085.
[10] Sheridan, B., Bagheri, M. and Rezania, M., 2024. Thermal creep and stress relaxation of London clay. *International Journal of Geomechanics*, *24*(4), p.04024043.
[11] Hueckel, T. and Baldi, G., 1990. Thermoplasticity of saturated clays: experimental constitutive study. *Journal of geotechnical engineering*, *116*(12), pp.1778-1796.
[12] Collins, I.F. and Kelly, P.A., 2002. A thermomechanical analysis of a family of soil models. *Géotechnique*, *52*(7), pp.507-518.
[13] Abuel-Naga, H.M., Bergado, D.T., Bouazza, A. and Ramana, G.V., 2007. Volume change behaviour of saturated clays under drained heating conditions: experimental results and constitutive modeling. *Canadian Geotechnical Journal*, *44*(8), pp.942-956.
[14] Laloui, L. and Cekerevac, C., 2008. Non-isothermal plasticity model for cyclic behaviour of soils. *International journal for numerical and analytical methods in geomechanics*, *32*(5), pp.437-460.
[15] Zhou, C. and Ng, C.W.W., 2015. A thermomechanical model for saturated soil at small and large strains. *Canadian Geotechnical Journal*, *52*(8), pp.1101-1110.
[16] Zymnis, D.M., Whittle, A.J. and Cheng, X., 2019. Simulation of long-term thermo-mechanical response of clay using an advanced constitutive model. *Acta Geotechnica*, *14*, pp.295-311.
[17] Li, Y., 2019. *On the impact of temperature perturbations on the creep of sensitive clay*. Chalmers Tekniska Hogskola (Sweden).
[18] Cheng, X., Li, Y., Karstunen, M., Dijkstra, J. and Abed, A., IMPLEMENTATION OF A NEW THERMO-VISCOPLASTIC SOIL MODEL USING FENICS PLATFORM.
[19] Srivastava, R. and Yeh, T.C.J., 1991. Analytical solutions for one-dimensional, transient infiltration toward the water table in homogeneous and layered soils. *Water Resources Research*, *27*(5), pp.753-762.
[20] Gras, J.P., Sivasithamparam, N., Karstunen, M. and Dijkstra, J., 2018. Permissible range of model parameters for natural fine-grained materials. *Acta Geotechnica*, *13*, pp.387-398.
[21] Abed, A.A. and Sołowski, W.T., 2017. A study on how to couple thermo-hydro-mechanical behaviour of unsaturated soils: Physical equations, numerical implementation and examples. *Computers and Geotechnics*, *92*, pp.132-155.
[22] Logg, A., Mardal, K.A. and Wells, G. eds., 2012. *Automated solution of differential equations by the finite element method: The FEniCS book* (Vol. 84). Springer Science & Business Media.
[23] Abed, A., Gerolymatou, E. and Karstunen, M., 2023. FEniCS simulation of a partially saturated slope under varying environmental loads. In *Proceedings 10th European Conference on Numerical Methods in Geotechnical Engineering (London)*.
[24] Maiullari, D., Nageli, C., Rudena, A. and Thuvander, L., 2023, November. Gothenburg Digital Twin. Modelling and communicating the effect of temperature change scenarios on building demand. In *Journal of Physics: Conference Series* (Vol. 2600, No. 3, p. 032006). IOP Publishing.
[25] Campanella, R.G. and Mitchell, J.K., 1968. Influence of temperature variations on soil behavior. *Journal of the Soil Mechanics and Foundations Division*, *94*(3), pp.709-734.
[26] Di Donna, A. and Laloui, L., 2015. Response of soil subjected to thermal cyclic loading: experimental and constitutive study. *Engineering Geology*, *190*, pp.65-76.